Mitochondrial Fatty Acid Oxidation is Stimulated by Red Light Irradiation

Manuel Alejandro Herrera, Camille C. Caldeira da Silva, Mauricio S. Baptista*, Alicia J. Kowaltowski*

[1]Departamento de Bioquímica, Instituto de Química, Universidade de São Paulo, Av. Prof. Lineu Prestes, 748, 05508-900, São Paulo, Brazil

*Corresponding authors: alicia@iq.usp.br, baptista@iq.usp.br

Abstract

The skin is our largest organ, and also the most exposed to solar radiation. As mitochondria within skin cells are rich in endophotosensitizers such as NADH, $FADH_2$, and cytochromes, we studied the effects of different UV and visible light wavelengths on metabolic fluxes in keratinocytes, the main cell type in the epidermis. We find that 36 J/cm^2 of UV light (λ_{max} at 365 nm) leads to a complete inhibition of oxidative phosphorylation. The same light dose at other wavelengths (blue light, 450 nm, and green light, 517 nm) did not affect metabolic fluxes, but reduced cell viability, probably by photosensitizing oxidation. Strikingly, red light (660 nm) not only did not decrease cell viability, but also enhanced cell proliferation as well as basal and maximal oxygen consumption rates for up to two days after irradiation. To uncover the mechanisms in which this unexpected long-lived metabolic enhancement occurred, we measured quantities of oxidative phosphorylation-related proteins and oxygen consumption in permeabilized cells, which were unchanged. This result is indicative of a modulation of cytosolic metabolic processes by red light. Subsequently, we measured glycolytic, glutamine-dependent, and fatty-acid supported metabolic fluxes and determined that red light specifically activates fatty acid oxidation by mitochondria. Overall, our results demonstrate that light modulates oxidative phosphorylation with different effects at distinct wavelengths. Interestingly, we uncover a novel and highly specific effect of red light modulating fatty acid oxidation in keratinocytes, providing a novel mechanistic explanation for the metabolic effects of photobiomodulation.

Highlights

Different UV and visible light wavelengths affect keratinocytes distinctly: UV leads to cell death and metabolic flux inhibition, while green light decreases viability without affecting oxygen consumption.

Surprisingly, red light increases intact cell oxygen consumption up to two days post exposure.

Red light exposure does not change the quantity or activity of components of oxidative phosphorylation in mitochondria.

Increased mitochondrial respiration and ATP synthesis promoted by red light is fueled by enhanced fatty acid oxidation.

1. Introduction

Living organisms evolved mechanisms to sense and respond to environmental stimuli [1], including light [2, 3], and specifically wavelengths emitted from the sun in the ultraviolet (UV, 320 to 400 nm) and visible light (400 to 700 nm) ranges [4]. Energy from the photons in both the UV and visible ranges can interact with different biomolecules scattering, transmitting, reflecting or absorbing light according to the optical properties of the components of that specific organism. The most recognized consequence of photon absorption is the generation of excited states, which are much more reactive than their ground states [4] and can interact with surrounding molecules, exciting other molecules and promoting chain reactions that may oxidize others (photosensitized oxidation) [5], a common undesirable effect of light.

The tissue most exposed to solar radiation in the human body is the skin, which is also our largest organ, vital in the maintenance of our body, offering an effective barrier against external agents, among many other functions. The skin involves a large number of cell types with different functions and relative abundance depending on the skin layer; in the epidermis, the most exposed layer to radiation, keratinocytes are the most common [6]. Indeed, endogenous photosensitizing molecules in keratinocytes such as flavins, nicotinamides, and cytochromes, located mostly in mitochondria, can produce excited and reactive species, affecting keratinocyte and skin function in response to light [7].

Interestingly, light exposure also has benefits to humans. Several light-based technologies are used to treat a variety of diseases, including photobiomodulation, in which light at different wavelengths is used to irradiate human skin, causing several beneficial effects, including pain control and wound healing, that can be useful in the treatment of inflammatory, neurological, and musculoskeletal disorders [8]. Although the molecular mechanisms responsible for the photobiomodulation are not completely understood, mitochondrial functions such as oxidative phosphorylation are often found to play an important role [9].

Indeed, mitochondria are pivotal for cell homeostasis as the center for energy metabolism, as well as having roles in cell growth, adaptation, death, ion homeostasis,

oxidant production, and thermogenesis, among others [10]. Many of these functions, and especially the canonic function of oxidative phosphorylation, require endophotosensitizers such as NADH, $FADH_2$, and metal-containing proteins and cytochromes in respiratory complexes I, III, and IV [11]. As a result, mitochondria and oxidative phosphorylation are an expected target of cellular functional consequences of light exposure.

Here, we questioned if, in addition to promoting melanogenesis [12], different wavelengths of light can affect oxidative phosphorylation and metabolic fluxes in keratinocytes. By studying metabolic fluxes, we were able to pinpoint specific light wavelengths that affect oxidative phosphorylation and cell integrity, promoting cell damage. Conversely, we find that the same dosage of red light promoted enhanced oxidative phosphorylation through an unexpected and novel mechanism, involving enhanced fatty acid oxidation.

2. Material and Methods

2.1. Cell Cultures

A human immortalized keratinocyte cell line (HaCaT, [13]) was cultured in high glucose Dulbecco modified eagle medium (DMEM) with phenol red (Gibco, Life Technologies, USA), supplemented with 10% v/v fetal bovine serum (FBS; Sigma), 110 mg/mL sodium pyruvate, 4 mM L-glutamine, 100 U/mL of penicillin, and 100 pg/mL of streptomycin (Gibco, Life Technologies, USA) at pH 7.4, 37°C in a humidified atmosphere of 5% CO_2. Passages were kept between 20 and 30, using 0.25% trypsin-EDTA for enzymatic dissociation. Cells were counted manually in a hemocytometer in the presence of trypan blue. Notably, primary keratinocytes undergo major metabolic alterations during and after isolation [14], justifying the use of a cell line.

2.2. Irradiation Sources and Conditions

Irradiation conditions for different wavelengths were adjusted by dose to a final 36 J/cm^2. For UVA, this was achieved with 6.57 mW/cm^2 at 365 nm λ_{max} (light source from

Biolambda, Brazil), for blue light with 31.02 mW/cm^2 at 450 nm λ_{max} (light source from Biolambda, Brazil), for green-light with 25.30 mW/cm^2 at 517 nm λ_{max} (light source from Biolambda, Brazil), and for red light with 24.90 mW/cm^2 at 660 nm λ_{max} (light source from Ethik Technology, Brazil). LED spectrum emissions used are presented in Supplementary Figure S1. Characterization of the emission sources was performed by acquiring emission spectra using a USB2000 + UV-VIS-ES spectrometer and a QP50–2-UV-VIS (Ocean Optics, USA) optical fiber. Irradiance was measured using a Laser Power Meter (Coherent Inc., Santa Clara, CA, USA) containing a silicon power sensor for the visible range (LM-2 Vis, 1,061,323). HaCaT cells were plated 24 hours before the experiment. Prior to irradiation treatment, they were washed and incubated in phosphate buffer saline (PBS), in an irradiation chamber without CO_2, and with controlled temperatures of 37°C. All treatments were done in PBS and in the chamber for the same time, including dark controls.

2.3. Cell Survival Assays:

2.3.1. MTT assay

Cell survival was estimated based on the reduction of 3-(4,5-dimethylthiazol-2-yl)-2,5-diphenyltetrazolium bromide (MTT). Exponentially growing HaCaT cells were plated (5×10^4 cells/well) in 48 well cell culture plates (Corning Costar) for 24 h. After 2, 48, and 72 hours of the treatment, we added 0.5 mL of medium containing MTT (Sigma, 50 µg/mL) to each well and incubated at 37°C for 3 h. The medium with MTT was then removed and 0.25 mL dimethyl sulfoxide (DMSO; Sigma) was added. The plate was shaken and absorbance values were read at 550 nm using a microplate reader (Expectramax i3, Molecular Devices, USA) with a wavelength correction set at 550 nm. Backgrounds in wells without cells were determined and subtracted.

2.3.2. Cristal Violet staining

Cell survival was also estimated by the accumulation of crystal violet (CV) in fixed cells. Exponentially-growing HaCaT cells were plated (5×10^4 cells/well) in 48 well cell culture plates (Corning Costar) for 24 h. After red light treatments (2, 48, and 72 hours), cells were washed twice with PBS, fixed in alcoholic-based 1.0% v/v acetic acid for 10 min,

washed twice with PBS and stained with CV (Sigma) at 0.02% w/v for 5 min at room temperature. After staining, cells were washed again with PBS to eliminate the non-ligated CV. CV was then eluted in 0.1 M sodium citrate - 50% v/v ethanol. Absorbance was read using the Espectramax i3 at 585 nm with a wavelength correction set at 585 nm for the subtraction of backgrounds in wells without cells.

2.3.3. Neutral Red incorporation assay

Cell survival was further estimated by accumulation of Neutral Red (NR), which dyes lysosomes in intact viable cells. Exponentially growing HaCaT cells were plated (5×10^4 cells/well) in 48 well cell culture plates (Corning Costar, cod. 3548) for 24 h. After red light treatment (2, 48, and 72 hours), cells were washed twice with PBS and stained with 30 µg/mL NR (Sigma) at 37°C for 2 h and subsequently washed twice with PBS. NR was eluted with an alcoholic-based 1.0% v/v acetic acid fixing solution for 10 min at room temperature and measured at 540 nm using an Expectramax microplate reader with wavelength correction set at 540 nm for subtraction of backgrounds in wells without cells.

2.4. Extracellular Metabolic Flux Analysis

2.4.1. Cell plating and irradiation

Cells were seeded at 1.5 $x10^5$ cells per well on Agilent Seahorse XF24 cell culture microplates in 500 µL high glucose DMEM with 10% FBS, 1% Penicillin/Streptomycin, without phenol red, and allowed to adhere overnight. Plates were treated with light in the absence of CO_2, after which the cells were returned to the CO_2 the incubator for 2 hours of recovery. Post-recovery time, cells were washed twice with 500 µL high glucose DMEM containing 1% penicillin/streptomycin. Media did not contain bicarbonate or FBS. Cells were kept for 1 h in a humidified incubator at 37°C without CO_2, after which Oxygen Consumption Rates (OCR) were measured using a Seahorse Extracellular Flux Analyzer (Agilent Technologies).

2.4.2. Mito-Stress test

After the preparation phase described above and incubation in bicarbonate-free media, plates were placed in the Seahorse Extracellular Flux Analyzer and OCR were measured under basal conditions, followed by injections of: a) oligomycin (final concentration 1 μM); b) CCCP (final concentration 1 μM); c) rotenone and antimycin (R/AA, 1 μM each final concentration). Unless otherwise specified, measurements were conducted with 3 min mixing + 1 min waiting + 2 min of measurements. Cell-free wells were incubated with the same medium for background correction, calculated by subtracting changes observed from the experiments in the presence of cells. OCR values obtained were normalized per amount of total protein in each well. For that, at the end of each experiment, the medium was removed, cells were PBS-washed, lysed with RIPA buffer, and total protein was quantified using the Pierce BCA Protein Assay kit.

2.4.3. Fatty acid and glutamine-supported OCRs

After the preparation phase described in 2.4.1 and incubation in bicarbonate-free media, Seahorse XF24 plates were placed in the equipment and OCRs were measured under basal conditions, followed injections of: a) etomoxir (final concentration 40 μM) or BPTES (final concentration 7 μM) or the same volume of DMEM in control wells; b) oligomycin (final concentration 1 μM); c) Carbonyl cyanide m-chlorophenyl hydrazone (CCCP, final concentration 1 μM); d) antimycin and rotenone (R/AA, 1 μM final concentration each). Measurements were conducted and normalized as described in 2.4.2.

2.4.4. Glycolysis stress test

Post-recovery from irradiation, cells were washed twice with 500 μL DMEM with no phenol red containing 1% penicillin/streptomycin. Media did not contain bicarbonate nor FBS. Cells were kept for 1 h in a humidified incubator at 37°C without CO_2. After incubation, Extra-Cellular Acidification Rates (ECARs) were measured using a Seahorse Extracellular Flux Analyzer (Agilent Technologies) under basal conditions, followed injections of: a) glucose (final concentration 25 mM); b) oligomycin (final concentration 1 μM); c) 2-deoxy-

glucose (2DG, final concentration 50 mM). Measurements were conducted and normalized as described in 2.4.2.

2.5. High Resolution Respirometry

Cells at 80% confluence were treated with red light at 0 J/cm^2 and 36 J/cm^2 and submitted to a recovery period as described in 2.4.1. Cells were then detached from the plate using 0.25% trypsin-EDTA, counted in a Countess 3 Cell Counter (Invitrogen, USA) in the presence of trypan blue. Oxygen consumption was measured using a high-resolution Oxygraph-2k (O2k) respirometer (Oroboros Instruments, Austria). One million cells were incubated in 1 mL of experimental buffer (250 mM sucrose, 100 μM EGTA, and 1 mg/mL bovine serum albumin) and different substrates described in the legend at 37°C with continuous stirring (400 rpm) with the light off in both chambers. After initial respiration was measured (state 2), state 3 respiration was measured by adding 1 mM ADP, followed by addition of 1 μM oligomycin (state 4), and 1 μM CCCP (state 3u). Respiratory control ratios (RCRs) were calculated as state 3/state 4.

2.6. Long-Term OCR Measurements

To measure metabolic effects of red light long-term, we followed OCRs in plated cells in CO_2 incubators under normal culture conditions using a Resipher Real-time Cell Analyzer (Lucid Scientific, Atlanta, GA, USA) for 3 days. 1 x 10^5 cells per well were cultured in a 96 Well black / clear Bottom (Corning Costar) plate using high DMEM without phenol (25 mM glucose, 10% FBS) and allowed to adhere overnight. The cell plates were treated with different doses of red light (0, 6, 12, 36 and 150 J/cm^2) and the Resipher sensor system was immediately placed above the plate. Measurements of basal OCRs were followed over three consecutive days in culture, in five technical replicates. Cell-free wells were included with the same media for background correction. Media was changed daily.

2.7. Western Blots

In order to quantify the expression of the electron transport chain and oxidative phosphorylation machinery, we performed Western blot analysis of the five oxidative phosphorylation complexes in cells treated with red light at 80% confluence. Cells were lysed

over ice in the presence of RIPA buffer containing protease and phosphatase inhibitor cocktails, and total protein levels were quantified using the Pierce BCA Protein Assay kit. Lysates were prepared in sample buffer (2% SDS, 10% glycerol, 0.062 M Tris pH 6.8, 0.002% bromophenol blue, 5% 2-mercaptoethanol), loaded onto 12% SDS-PAGE, and electro-transferred to PVDF membranes. Membranes were blocked with 5% BSA in TTBS (20 mM Tris pH 7.5, 150 mM NaCl, and 0.1% Tween 20) for 1 h at room temperature before overnight incubation with Total OXPHOS Human WB Antibody Cocktail (ab110411, 1:1000) primary antibody at 4°C. Fluorescent 660 nm secondary Anti-mouse antibody (1:20.000) was incubated for 1 h at room temperature prior to fluorescence detection using a ChemiDoc Imaging System (Bio-Rad). Quantification of band densitometry was performed using the ImageLab software. Given that no single protein is a strong housekeeping control in metabolism, protein expression values obtained were normalized per pixels of total protein in each well, as evidenced by Ponceau S dye (Sigma).

2.8. Statistical Analysis

Data shown in graphs are individual biological replicates, averages, and standard deviations. Statistical analysis was carried out using GraphPad Prism 8 Software for at least three independent experiments (biological replicates). Student's t test was used to compare differences between treated and untreated conditions in high resolution respirometry results. One-way ANOVA followed by Tukey or Dunnet was used to compare multiple conditions with one independent variable with confidence levels set to $p < 0.05$.

3. Results

3.1. Effects of light on keratinocyte viability is dependent on wavelength

To initially assess the effect of UVA and visible light on keratinocytes, we selected the midpoints of the spectra (i.e., 365 nm, 450 nm, 517 nm, and 660 nm, see Supplementary Figure S1 for spectra) and submitted cells to one dose of 36 J/cm² at each wavelength. Viability was measured using MTT, Cristal Violet Staining (CVS), and neutral red staining (NRS), so as not to incur on specific light effects on the specific processes assessed by each

of these dyes (Fig. 1). UVA exposure resulted in loss of cell viability 48 hours after exposure as measured by all methods (Fig. 1A-C), an effect maintained 72 hours post treatment (Fig. 1D-F) and compatible with prior findings [17]. Blue light had no detectible effect compared to non-irradiated controls. Interestingly, green light promoted a decrease in MTT and CVS at 48 hours (Fig. 1A-B) and 72 hours (Fig. 1D, E), which indicates that 36 J/cm^2 of green light inhibits keratinocyte growth. Conversely, red light-treated cells displayed enhanced CVS intensity, suggesting it increased proliferation at 48 hours (Fig. 1B) and 72 hours post treatment (Fig. 1E). Overall, the results in Fig. 1 indicate that keratinocytes respond differently to the same dose of light at distinct wavelengths, with responses ranging from overt cell death (UVA light) to augmented cell counts (red light).

3.2. Metabolic fluxes are affected by different light wavelengths

To investigate the implications of light on electron transport and oxidative phosphorylation, an expected target of irradiation due to their dependence on various light-absorbing molecules, we measured metabolic fluxes through OCR in intact cells exposed to 36 J/cm^2 of different wavelengths of light. Intending to uncover metabolic changes induced early on in cells, OCRs were measured 2 hours post irradiation in plated cells using a Seahorse Extracellular Flux Analyzer (Fig. 2). Figure 2A shows typical intact cell OCR measurements over time. Measurements were made under basal conditions (prior to any additions) and reflecting the normal metabolic status of the cells (quantified in Fig. 1B). oligomycin, an ATP synthase inhibitor, was then added to quantify OCRs dependent on mitochondrial oxidative phosphorylation (quantified in Fig. 1C). Maximal electron transport was then induced by adding the uncoupler CCCP (quantified in Fig. 1D), followed by antimycin and rotenone to inhibit mitochondrial electron transport and determine non-mitochondrial OCRs, which were subtracted from all quantifications.

Compared to controls (gray lines/bars), we found that UVA irradiation almost completely abrogates OCRs (Fig. 2A-D), a result compatible with the loss of viability seen in Fig. 1. Blue and green light promoted no changes in basal (Fig. 2B), ATP production-linked (Fig. 2C), or maximal respiration (Fig. 2D). Interestingly, keratinocytes presented a substantial increase in all OCRs states when treated with red light: basal respiration (Fig. 2B), ATP production (Fig. 2C), and maximal respiration (Fig. 2D) were enhanced,

demonstrating that red light significantly increases oxidative phosphorylation and electron transport capacity. Extracellular acidification rates (ECARs) and OCRs associated to the proton leak, reserve capacity and non-mitochondrial respiration were equal between all treatments, except for enhancements promoted by red light (Supplementary Fig. S2). Overall, we find that metabolic fluxes in intact cells are impacted by light differentially depending on wavelengths, with a highly interesting enhanced basal, ATP-linked, and maximal oxygen consumption observed after red light irradiation.

3.3. Red light increases oxidative phosphorylation within a physiological dose range, with long-lasting effects

We then sought to better characterize the enhancement of oxidative phosphorylation seen with red light, and tested if different doses of 660 nm irradiation had similar effects (Fig. 3). We found that increasing exposure up to 36 J/cm^2 enhanced OCRs dose-dependently, but that a higher exposure of 150 J/cm^2 decreased OCRs, probably due to a toxic effect. Importantly, red light doses between 5 and 150 J/cm^2 are compatible with typical human exposure and with photobiomodulation protocols [7, 15], indicating that the modulatory effects seen here could constitute a physiological response *in vivo*.

As we had measured a single time point (two hours after irradiation) so far, we sought next to uncover the timeline of the enhanced oxygen consumption rates observed in our cells. For this, we used a Resipher Real-time Cell Analyzer (Lucid Scientific, Atlanta, GA, USA), capable of measuring oxygen consumption in plated cells within normal growth conditions in normal laboratory CO_2 incubators. Cells were plated under conditions similar to those used in the Seahorse metabolic flux experiments, except that OCRs were quantified continuously immediately after a single bought of red-light exposure at different intensities (Fig. 4). We found that oxygen consumption rates became elevated soon after irradiation, in a dose-dependent manner, a result compatible with the Seahorse data, although higher, 150 J/cm^2 doses also elevated OCRs in this setting, possibly due to the presence of bicarbonate (the only discernable experimental difference between experimental setups). Surprisingly, this effect was long-lasting, and maintained for over 2 days, irrespective of daily changes in culture media, which were accompanied by a temporarily decreased OCR. Starting at day 3 post-irradiation, OCRs were again similar in irradiated and non-treated groups. The finding

that red light enhancement of oxygen consumption rates and capacity is long-lasting is interesting, and suggests mechanisms other than direct light interactions with mitochondrial molecules.

3.4. Red light does not alter mitochondrial oxidative phosphorylation machinery

We sought next to identify the mechanisms in which red light promotes long-lasting enhanced oxygen consumption rates. We began by analyzing the quantities of respiratory-protein complexes (OXPHOS complex subunits) by western blot (Fig. 5), and observed no changes in the Complex I – NADH dehydrogenase (I-NDUFBS), Complex II – Succinate dehydrogenase (SDHB), Complex III - Q-cytochrome c oxidoreductase (III-UQCRC), Complex IV – cytochrome C oxidase (IV-COX II) or Complex V - ATP Synthase (V-ATP5A), relative to the dark control.

The activity of oxidative phosphorylation components may be altered independently of their expression. Indeed, some groups have suggested that red light directly activates cytochrome c oxidase [15, 16]. While our finding that the effects of red light are long-lasting is not compatible with this mechanism (which would require the presence of light during measured activation), we decided to measure electron transport rates more directly in permeabilized cells (Fig. 6), in which cytoplasmic factors are infinitely diluted, allowing us to directly probe mitochondrial oxygen consumption regulation using a Clark-type high resolution respirometer (Oroboros Oxygraph-2k). Oxygen consumption supported by a physiological mixture of substrates was measured under initial basal conditions and after the addition of ADP (which stimulated oxidative phosphorylation), oligomycin (which inhibits oxidative phosphorylation), and CCCP (which promotes uncoupling and maximizes electron transport). Respiratory control ratios (ADP-induced/oligomycin-treated OCRs) were also calculated. None of these parameters were significantly altered by red light. This clearly indicates that the respiratory enhancement observed in intact cells is not centered on a mitochondrial regulatory mechanism, and probably therefore involves modulation of cytosolic metabolic pathways upstream of oxidative phosphorylation.

3.5. Red light irradiation specifically enhances fatty acid oxidation in keratinocytes

Since mitochondrial OCRs were equal in irradiated and control cells when substrates were delivered directly to the organelles of permeabilized cells, but enhanced by light in intact cells, we investigated if cytosolic pathways fueling mitochondrial oxidative phosphorylation were affected by red light.

Glucose metabolism was dynamically assessed first, by quantifying proton release dependent on glucose degradation and enhanced by oligomycin, an ATP synthase inhibitor which promotes ATP depletion and activates the pathway (Fig. 7). By following ECARs over time after the additions of glucose, oligomycin and the competitive inhibitor 2-deoxiglucose (Fig. 7A), we were able to quantify basal (Fig. 7B), maximal (Fig. 7C), and reserve (Fig. 7D) glycolytic rates in irradiated and control cells, as well as non-glycolytic acidification rates (Fig. 7E). Results clearly show that there is no effect of red light, as none of these parameters are significantly altered.

Next, we measured the effect of red light on amino acid metabolism, by following the effect of BPTES, a glutaminase inhibitor, on OCRs in the presence and absence of red light. BPTES was added to control or red light-irradiated keratinocytes, and OCRs were followed over extended time to allow for glutaminase inhibition (Fig. 8A). Basal, maximal, and ATP-linked respiration were enhanced by red light, but this effect was not abrogated by BPTES, indicating that it does not involve a change in glutaminase activity (Fig. 8B-E).

Next, we measured oxygen consumption promoted by fatty acid oxidation (FAO), specifically long-chain fatty acids, which are the main lipid energy source in mammalian cells. To measure FAO-dependent metabolic fluxes, we compared OCRs before and after the addition of etomoxir, an inhibitor of CPT1, which transports fatty acids into mitochondria, where they are degraded by fatty acid oxidation. Similarly to CCCP and oligomycin, the use of etomoxir was preceded by careful calibration experiments to determine ideal quantities and avoid off-target effects such as uncoupling (which increases OCRs in the presence of oligomycin). Using calibrated etomoxir quantities, we found that OCRs were decreased by etomoxir over time specifically in red light-irradiated cells (Fig. 9), while inhibition of FAO had a non-significant effect on control cells. Indeed, etomoxir abrogated the stimulated basal

and maximal OCRs observed in red light-irradiated cells, indicating that increased CPT1-dependent FAO is the mechanism in which red light promotes enhanced oxygen consumption in intact cells.

4. Discussion

Exposure to light is a part of everyday life, and therefore an important aspect to understand scientifically. Historically, light exposure has always been associated with phototoxicity promoted by UVA and UVB light, but more recently visible light ranges such as blue light have also been found to have significant biological effects [17]. In general, most of the biological effects of light described to date are damaging to cells and involve photosensitizing, which generates excited species such as singlet oxygen [5], radicals such as nitric oxide [18] and hydroxyl radicals [19]. This leads to oxidation of important biomolecules including lipids, nucleic acids, and proteins, which can result in unwanted consequences of sunlight exposure such as erythema, photoaging, and cancer.

Given that keratinocytes are the most abundant cell type in the epidermis and that, like all cells, they are rich in endo-photosensitizers, molecules capable of converting light energy into chemical energy by transferring energy or electrons to molecular substrates, we studied here the effects of irradiation with different wavelengths present in sunlight on these cells. We specifically targeted understanding the effects of light on metabolic fluxes, since energy metabolism, and particularly mitochondria, involve high quantities and variety of endo-photosensitizers. Our results confirm that 365 nm UVA exposure at a dose of 36 J/cm^2 is markedly cytotoxic, leading to both a loss in cell viability (Fig. 1) and abrogated electron transport and oxidative phosphorylation (Fig. 2). Indeed, other groups have found that oxidative imbalance occurs in keratinocytes submitted to UV light [20, 21]. DNA oxidation is one of the targets of photo-oxidation, generating adducts like 8-oxo-7,8-dihydroguanine, which may generate molecular responses such as mutations and, inflammation [22].

Blue light (450 nm) is another wavelength which should be considered when analyzing the cellular effects of sunlight. Indeed, $NAD(P)^+$ and NAD(P)H absorb in the blue

light range [7] and within membrane compartments can accelerate photosensitized NADH to NAD^+ conversion [23]. Metabolically, blue light promotes a reduction in maximal respiratory capacity in retina cells [24], as well as increased inflammatory response [25]. Prior studies in retinal cells also find that blue light irradiation at 445 nm correlated with dysregulation of protein levels associated with mitochondrial morphology and dynamics [26]. In epithelial cells, blue light promoted damage to mitochondrial DNA and oxidant production [27]. In keratinocytes, at a dose of 36 J/cm^2, we find no effect of blue light on viability (Fig. 1) or metabolic fluxes (Fig. 2). This is compatible with prior results from our group showing that blue light affects keratinocyte viability at does of 60 J/cm^2 and over [17].

Green light can affect molecules that absorb in this range such as flavins [28, 29]. Indeed, retinal cells have been shown to present decreased viability and electron transport promoted by green light (517 nm, [18, 24]). In adipose cells [30], green light promoted oxidative imbalance related to activation of TRPV1 channels, increasing calcium ion transport. On the other hand, [31] irradiation at 516 nm induces endothelial cell proliferation. Lunova et al., [32] found that irradiation at 502 nm did not promote any effect on inner mitochondrial membrane potentials in hepatic cells, a result that is compatible with our finding that green light did not change basal, ATP-linked, nor maximal mitochondrial electron transport in keratinocytes (Fig. 2), although this wavelength did promote a moderate decrease in cell viability (Fig. 1), through mechanisms that do not involve changes in oxidative phosphorylation.

While damaging effects of light are described in many cells, and expected given spectral properties, we were surprised to see a significant enhancement in basal, ATP-linked and maximal oxygen consumption rates in keratinocytes two hours after being irradiated with red light (660 nm, Fig. 2), an effect that was accompanied by enhanced cell proliferation 48 and 72 hours post-irradiation (Fig. 1). Our results are compatible with those of [33], who found that an epidermal-equivalent cell model and human skin presented increased proliferation after red light treatment, with enhanced mitochondrial oxygen consumption in the cell model. The enhanced oxygen consumption observed occurred in the range of 12-36 J/cm^2 (Fig. 3), a dosage compatible with expected sunlight exposure [34]. Similarly, mesenchymal stem cells treated with 0.5 a 4 J/cm^2 red light (630 nm) had significantly

increased ATP production and interleukin secretion (IL-6 and IGF-1, [35]). Chu-tan et al., [36] observed an increase of spare respiratory capacity and non-mitochondrial respiration in retinal cells when irradiated with 670 nm red light at different doses. Chu-tan et al., [36] also observed a hormesis effect with low and high doses of light, where higher doses could induce phototoxic effects. This result is compatible with our results in keratinocytes, in which higher doses (150 J/cm^2) promoted decreased respiration (Fig. 3) and decreased clonogenicity (not shown).

The enhanced oxidative phosphorylation we see in keratinocytes is, therefore, compatible with prior results in the literature. Typically, these effects in prior publications have been associated with photo biomodulation-mediated activation of cytochrome c oxidase in mitochondria directly by red light [37]. However, our results are not compatible with a direct effect of red light on cytochrome c oxidase, for many reasons. First, results are present from two hours (Figs. 2 and 3) to two days (Fig. 4) after irradiation, which would be unexpected for a direct effect of light on enzymatic components. Second, red light increased both basal and maximal oxygen consumption rates (Figs. 2 and 3), while the expected result for cytochrome c oxidase activation in cells with robust reserve respiratory capacity (the difference between basal and maximal oxygen consumption) such as the keratinocytes studied here would be in an increase in maximal oxygen consumption alone. Indeed, the enhanced basal and maximal oxygen consumption rates in the absence of a change in oxygen consumption in the presence of the ATP-synthase inhibitor oligomycin, as observed by us here, suggests an increase in ATP demand and electrons arriving at the electron transport chain from upstream metabolic pathways. These results are in agreement with the observation that cell models lacking cytochrome c oxidase also show the typical photobiomodulation effect of enhancing cell proliferation after red-light irradiation [38].

Consistently, quantification of components of the machinery of oxidative phosphorylation showed no increase that was explanatory of the enhanced oxygen consumption rates observed in cells (Fig. 5). Interestingly, oxygen consumption rates measured in permeabilized cells, in which soluble cytosolic components are eliminated with preservation of mitochondrial morphology and metabolism, were equal in cells that were irradiated or not (Fig. 6), indicating the effect of red light was on cytosolic metabolic

pathways. Using intact cells and monitoring metabolic fluxes dependent on glycolysis (Fig. 7), glutaminase (Fig. 8), and fatty acid oxidation (Fig. 9), we were able to determine that red light irradiation specifically enhanced the latter. Indeed, etamoxir, an inhibitor of CPT1 and long chain fatty acid entry into mitochondria, specifically decreased respiration in red light-stimulated mitochondria and equalized respiratory rates to those of control cells, confirming that the enhancement is due to fatty acid uptake into mitochondria (Fig. 8). While the results involved completely different cell types, our finding that red light induces lipolysis in keratinocytes is compatible with red light treatment (635 nm) effects in rodents, in which it prevented weight gain, hyperlipidemia, and hepatic steatosis promoted by high fat diets [39]. Overall, the idea that red light may induce lipolysis at a cellular level and enhance basal metabolic rates as a result of this is a new and enticing effect of red light uncovered here.

5. Conclusions

Our work shows that keratinocyte viability and metabolism is affected by different wavelengths present in sunlight (see Fig. 10). Intriguingly, while UVA and green light decreased viability, and UVA completely abrogated metabolic fluxes, red light irradiation consistently enhanced oxygen consumption rates in these cells. The effect of red light was long-lasting and occurred at dosages that are compatible with normal exposure to the sun. Intriguingly, the effects of red light were not related to direct changes in mitochondrial metabolism, but instead to a specific enhancement of fatty oxidation in irradiated cells. This new and interesting effect of light may explain many of its effects in animal models, and expands the possibilities of use of red light in physiological cell modulations and therapeutics.

6. References

[1] T. C. Boothby, *EvoDevo* **2019**, *10***,** 30.

[2] G. H. Jacobs, *Visual Neuroscience* **2013**, *30*, 39.

[3] L. Walmsley, L. Hanna, J. Mouland, F. Martial, A. West, A. Smedley, D. Bechtold, A. Webb, R. Lucas, T. Brown, *PLOS Biology* **2015**, *13*, e1002127.

[4] E. Bastos, F. Quina, M. Baptista, *Chemical Reviews* **2023,** *123*, 9720.

[5] M. S. Baptista, J. Cadet, P. Di Mascio, A. A. Ghogare, A. Greer, M. R. Hamblin, C. Lorente, S. C. Nunez, M. S. Ribeiro, A. H. Thomas, M. Vignoni, T. M. Yoshimura, 2017. *Photochemistry and Photobiology* **2017,** *93*, 912.

[6] B. Dyring-Andersen, M. B. Løvendorf, F. Coscia, A. Santos, L. Pilgaard, A. Colaço, L. Niu, M. Bzorek, S. Doll. J. Lock, R. Clark, S. Skov, M. Teunissen, M. Mann, *Nature Communications* **2020,** *11*, 5587.

[7] L. V. de Assis, P. N. Tonolli, M. N. Moraes, M. Baptista, A. M. de Lauro Castrucci, *Journal of Photochemistry and Photobiology C: Photochemistry Reviews* **2021**, *47*, 1389.

[8] M. C. P. Felician, R. Belotto, J. P. Tardivo, M. S. Baptista, W. K. Martins, *Journal of Photochemistry and Photobiology* **2023,** *17*, 1.

[9] D. J. Davies, M. Hadis, V. Di Pietro, G. Lazzarino, M. Forcione, G. Harris, A.R. Stevens, W. C. Soon, P. Goldberg Oppenheimer, M. Milward, A. Belli, W. M. Palin, *PLoS One* **2022,** *17*.

[10] A.S. Monzel, J.A. Enríquez, M. Picard, *Nature Metabolism* **2023,** *5*, 546.

[11] D. Nicholls, S. Ferguson, Bioenergetics,4th ed., Academic press, Oxford **2013**

[12] Q. Wu, Y. Xia, K. Dai, P. Bai, K. K. L. Kwan, M. S. S. Guo, T. T. X. Dong, K. W. Tsim, *FASEB Journal* **2020**, *34*, 8941.

[13] A. Svobodová Ulrichová J. Vostálová, *Anais Brasileiros de Dermatologia* **2019**, *94*, 105.

[14] C. Kremslehner, A. Miller, R. Nica, I.M. Nagelreiter, M.S. Narzt, B. Golabi, V. Vorstandlechner, M. Mildner, J. Lachner, E. Tschachler, F. Ferrara, K. Klavins, M. Schosserer, J. Grillari, A. Haschemi, F. Gruber, *Redox Biology*, **2020**, *37*, 101583.

[15] Y. Y. Huang, A.C. Chen, J.D. Carroll, M.R. Hamblin, *Dose-Response* **2009,** *7*, 358.

[16] L. F. de Freitas, M.R. Hamblin, *IEEE Journal of Selected Topics in Quantum Electronics*, **2016**, *22*, 000417.

[17] P. N. Tonolli, C.M. Vera Palomino, H.C. Junqueira, M.S. Baptista, *Journal of Photochemistry and Photobiology B: Biology* **2023,** *243*, 112703.

[18] N. J. Pope, S.M. Powell, J.C. Wigle, *Journal of Biomedical Optics* **2020,** *25*, 085001.

[19] M. S. Baptista, J. Cadet, A. Greer, A.H. Thomas, *Photochemistry and Photobiology.* **2021** *97*, 1456.

[20] G. R. Aitken, J.R. Henderson, S.C. Chang, C.J. McNeil, M.A. Birch-Machin, *Clinical and Experimental Dermatology* **2007,** *32*, 722.

[21] J. Cadet, T. Douki, *Journal of Investigative Dermatology* **2011,** *131*, 1005.

[22] J. Cadet, T. Douki, J.L. Ravanat, *Photochemistry and Photobiology* **2015,** *91*, 140.

[23] R. E. P. Nau, J. Bösking, A. Pannwitz, *ChemPhotoChem* **2022**, *6*, 1.

[24] M. Marie, K. Bigot, C. Angebault, C. Barrau, P. Gondouin, D. Pagan, S. Fouquet, T. Villette, J. Sahel, G. Lenaers, S. Picaud, *Cell Death & Disease* **2018**, *9*, 1096.

[25] W. Song, R. Zhu, W. Gao, C. Xing, L. Yang, *Frontiers in Medicine* **2022,** *9*, 831463.

[26] A. Alaimo, G.G. Liñares, J.M. Bujjamer, R.M. Gorojod, S.P. Alcon, J.H. Martínez, A. Baldessari, H.E. Grecco, M.L. Kotler, *Archives of Toxicology* **2019**, *93*, 1401.

[27] B. F. Godley, F.A. Shamsi, F.Q. Liang, S.G. Jarrett, S. Davies, M. Boulton, *Journal of Biological Chemistry* **2005,** *280*, 21061.

[28] C. K. Remucal, K. McNeill, *Environmental Science & Technology* **2011**, *45*, 5230.

[29] K. Hirakawa, T. Yoshioka, *Chemical Physics Letters* **2015,** *634*, 221.

[30] Y. Wang, Y.Y. Huang, Y. Wang, P. Lyu, M.R. Hamblin, *Scientific Reports* **2017**, *7*, 1.

[31] S. Rohringer, W. Holnthoner, S. Chaudary, P. Slezak, E. Priglinger, M. Strassl, K. Pill, S. Mühleder, H. Redl, P. Dungel, *Scientific Reports* **2017,** *7*, 1.

[32] M. Lunova, B. Smolková, M. Uzhytchak, K. Ž. Janoušková, M. Jirsa, D. Egorova, A. Kulikov, Š. Kubinová, O. Lunov, *Cellular and Molecular Life Sciences* **2020,** *77*, 2815.

[33] Y. Umino, M. Denda, *Skin Research & Technology* **2023**, *29*, e13447.

[34] P. N. Tonolli, *Ph.D Degree Thesis*, Universidade de São Paulo, São Paulo, Brazil, **2018**. https://doi.org/10.11606/T.46.2018.tde-12122018-114252

[35] B. S. Dias-Martins, *Ph.D Degree thesis*, Universidade Nove de Julho, São Paulo, Brazil, **2020**.

[36] J. A. Chu-Tan, M. Rutar, K. Saxena, Y. Wu, L. Howitt, K. Valter, R. Natoli, *International Journal of Photoenergy* **2016,** *1*, 1.

[37] J. Maghfour, D.M. Ozog, J. Mineroff, J. Jagdeo, I. Kohli, H.W. Lim, *Journal of the American Academy of Dermatology* **2024,** *S0190-9622*.

[38] P. L.V. Lima, C.V. Pereira, N. Nissanka, T. Arguello, G. Gavini, C.M. Maranduba, F. Diaz, C.T. Moraes, *Journal of Photochemistry and Photobiology B: Biology* **2019,** *194*, 71.

[39] S. Guo, L. Gong, Q. Shen, D. Xing, *Journal of Photochemistry and Photobiology B: Biology* **2020,** *213*, 112075.

7. Figure Legends

Figure 1. The effect of light on cell viability in keratinocytes is dependent on wavelength. Cell viability was quantified after 48 Panels A-C) and 72 (Panels D-F) hours post-irradiation at 36 J/cm^2 with UVA (365 nm), blue light (450 nm), green light (517 nm), or red light (660 nm). Viability was assessed using MTT (A, D), Cristal Violet Staining (CVS, B, E), or neutral red staining (NRS, C, F), as indicated. ns = > 0.1. *p = <0.0332. **p = 0.0021. ***p = 0.0002 ****p = <0.0001. Results are expressed as means ± SD of three independent experiments; One-way ANOVA followed by Dunnett.

Figure 2. Mitochondrial respiration is differentially modulated by different light wavelengths. Cell oxygen consumption rates (OCR) were quantified after 2 hours irradiation at 36 J/cm^2 with UVA (365 nm), blue light (450 nm), green light (517 nm), or red light (660 nm). OCRs were measured as described in the methods section under basal conditions, followed by injection of oligomycin (oligo, 1 μM), CCCP (1 μM), and antimycin A plus rotenone (AA/Rot, 1 μM each). ns = > 0.1. *p = <0.0332. **p = 0.0021. ***p = 0.0002 ****p = <0.0001. Results are expressed as means ± SEM of three independent experiments; One-way ANOVA followed by Dunnett.

Figure 3. Moderate doses of red light (660 nm) increase mitochondrial respiration. OCRs were quantified under similar conditions to Fig. 2 after 2 hours irradiation at 6, 12,

36 and 150 J/cm^2 with red light. ns = > 0.1. *p = <0.0332. **p = 0.0021. ***p = 0.0002. ****p = <0.0001. Results are expressed as mean ± SD of three independent experiments; One-way ANOVA followed by Dunnett.

Figure 4. Increased oxygen consumption promoted by red light (660 nm) is prologued. OCRs were measured over three days in culture using a Resipher Real-Time Cell Analyzer under basal conditions. Cell respiration (OCR) quantification was initiated immediately post irradiation with red light at different doses (0, 6, 12, 36, and 150 J/cm^2), as indicated. Results are means + SEM of 4 biological replicates.

Figure 5. Red light does not change mitochondrial respiratory complex expression. Western blot analysis of electron transport chain and oxidative phosphorylation protein levels was conducted in cells 2 hours post exposure to red light at different doses (0, 6, 12, 36 and 150 J/cm^2). Extracts were collected and protein quantified by BCA. Complex I – NADH dehydrogenase (I-NDUFBS), Complex II – Succinate dehydrogenase (SDHB), Complex III - Q-cytochrome c oxidoreductase (III-UQCRC), Complex IV – Cytochrome C oxidase (IV-COX II) and Complex V - ATP Synthase (V-ATP5A). Results are means + SD of 3 biological replicates.

Figure 6. Effect of red light on mitochondrial oxidative phosphorylation requires intact cells. A: Permeabilized cells were incubated in the presence of 0.0017% digitonin, 1 mM succinate, 1 mM pyruvate, and 1 mM malate (state 2), 1 mM ADP (state 3), 1 μM oligomycin (Oligo, state 4), and 1 mM CCCP (state 3U), added successively, while oxygen consumption was monitored as described in the methods section. B: respiratory control ratios were calculated as the ratio between state 3 and state 4. Results are means + SD of 3 biological replicates.

Figure 7. Glycolysis is not affected by red light. ExtraCellular Acidification Rates (ECARs) were measured as described in Methods in intact cells 2 hours post irradiation at 36 J/cm^2 with red light (660 nm) under basal conditions, followed by injection of Glucose (Glc, 25 mM), Oligomycin (Oligo, 1 μM) and 2-Deoxy-Glucose (2DG, 50 mM). Results are expressed as means ± SD of three independent experiments; Student's t test, ns = > 0.1.

Figure 8. Glutamine oxidation is unaffected by red light. Oxygen Consumption Rates (OCR) sensitive to glutaminase inhibitor BPTES was analyzed 2 hours post irradiation at 36 J/cm^2 at 660 nm under basal conditions, followed by injection of BPTES (7 μM) oligomycin (oligo, 1 μM), CCCP (1 μM), and antimycin A/rotenone (AA/Rot, 1 μM each). ns = > 0.1. *p = <0.0332. Results are expressed as means ± SD of three independent experiments; One-way ANOVA followed by Dunnett.

Figure 9. Fatty acid oxidation is enhanced by red light. Oxygen Consumption Rates (OCR) sensitive to CPT1 inhibitor etomoxir were analyzed 2 hours post irradiation at 36 J/cm^2 at 660 nm under basal conditions, followed by injection of Etomoxir (40 μM), oligomycin (oligo, 1 μM), CCCP (1 μM), and antimycin A / rotenone (AA/Rot, 1 μM each). ns = > 0.1. *p = <0.0332. Results are expressed as means ± SD of three independent experiments; One-way ANOVA followed by Dunnett.

Figure 10. Light at different wavelengths has distinct effects on keratinocyte viability and metabolism. UVA light abrogates metabolic fluxes and cell viability. Blue and green light have no effect on metabolic fluxes, while red light enhanced oxidative phosphorylation by promoting fatty acid oxidation.

8. Supplementary Figure Legends

Figure S1. Spectral distributions of LEDs used for irradiation treatments: UVA (365 nm), blue light (450 nm), green light (517 nm), and red light (660 nm). Irradiance was measured as described in the methods section.

Figure S2. Mitochondrial respiration is differentially modulated by different light wavelengths. Cell oxygen consumption rates (OCR) and Extracellular Acidification Rates (ECAR) were quantified after 2 hours irradiation at 36 J/cm^2 with UVA (365 nm), blue light (450 nm), green light (517 nm), or red light (660 nm). OCRs/ECARs were measured as described in Methods under basal conditions, followed by injection of oligomycin (oligo, 1 μM), CCCP (1 μM), and antimycin A plus rotenone (AA/Rot, 1 μM each). ns = > 0.1. *p = <0.0332. **p = 0.0021. ***p = 0.0002 ****p = <0.0001. Results are means ± SEM of three independent experiments; One-way ANOVA followed by Dunnett.

Abbreviations

2DG: 2-deoxy-glucose; CCCP: Carbonyl cyanide m-chlorophenyl hydrazone; CV: crystal violet; CVS: Cristal Violet Staining; DMSO: dimethyl sulfoxide; ECAR: Extra-Cellular Acidification Rates; FAO: Fatty acid oxidation; FBS: fetal bovine serum; III-UQCRC: Q-cytochrome c oxidoreductase; I-NDUFBS: NADH dehydrogenase; IV-COX II: cytochrome C oxidase; MTT: 3-(4,5-dimethylthiazol-2-yl)-2,5-diphenyltetrazolium bromide; NR: Neutral Red; NRS: neutral red staining; OCR: Oxygen Consumption Rates; PBS: phosphate buffer saline; R/AA: rotenone and antimycin; RCR: Respiratory control ratios; SDHB: Succinate dehydrogenase; V-ATP5A: ATP Synthase

Author contributions

All authors participated in experimental design, data analysis, reading and approval of the final manuscript. MAHL and CCCS conducted experiments.

Conflict of interest

The authors declare that they have no conflicts of interest with the contents of this article.

Acknowledgments

This work was supported mainly by the Fundação de Amparo à Pesquisa do Estado de São Paulo (FAPESP) Supported by the Fundação de Amparo à Pesquisa do Estado de São Paulo (FAPESP) grant numbers 20/06970-5 and 2021/08521-6, Conselho Nacional de Pesquisa e Desenvolvimento (CNPq), Coordenação de Aperfeiçoamento de Pessoal de Nível Superior (CAPES) line 01 and the Centro de Pesquisa, Inovação e Difusão de Processos Redox em Biomedicina - CEPID Redoxoma, grant 2013/07937-8. MAHL is supported by a FAPESP fellowship. We thank Helena C. Junqueira for excellent technical assistance.

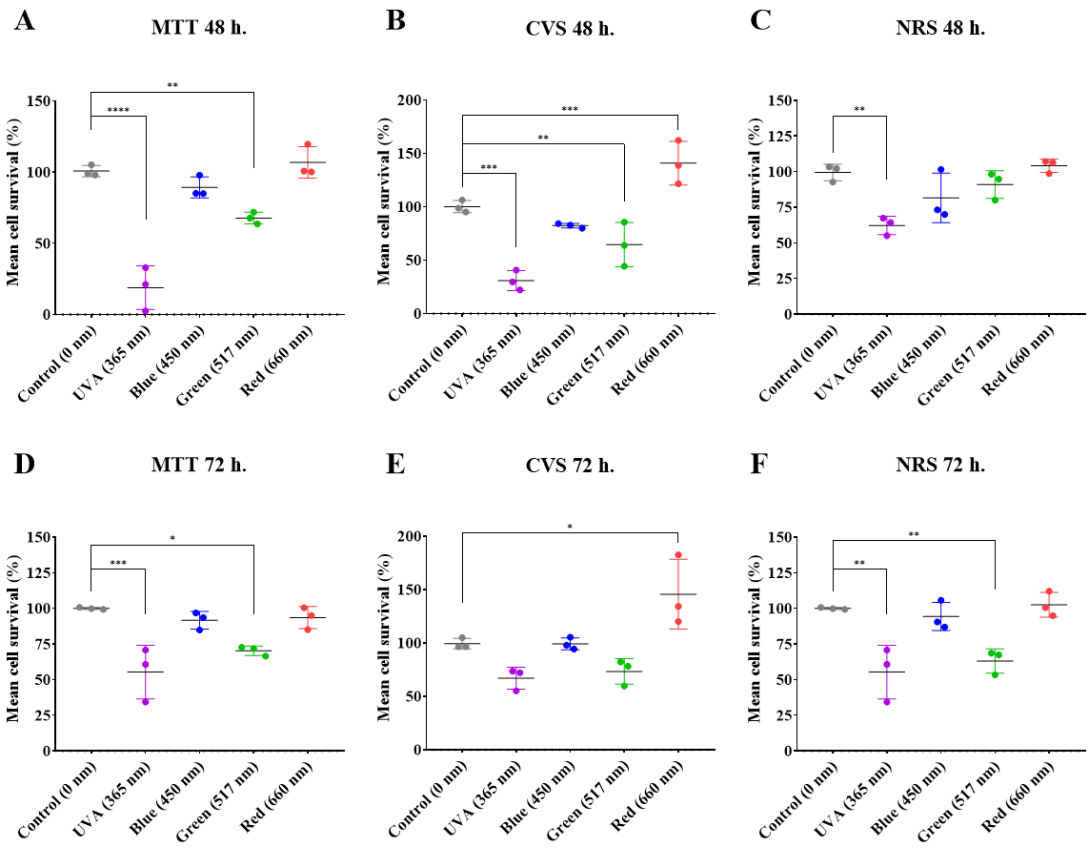

Herrera et al., Figure 1

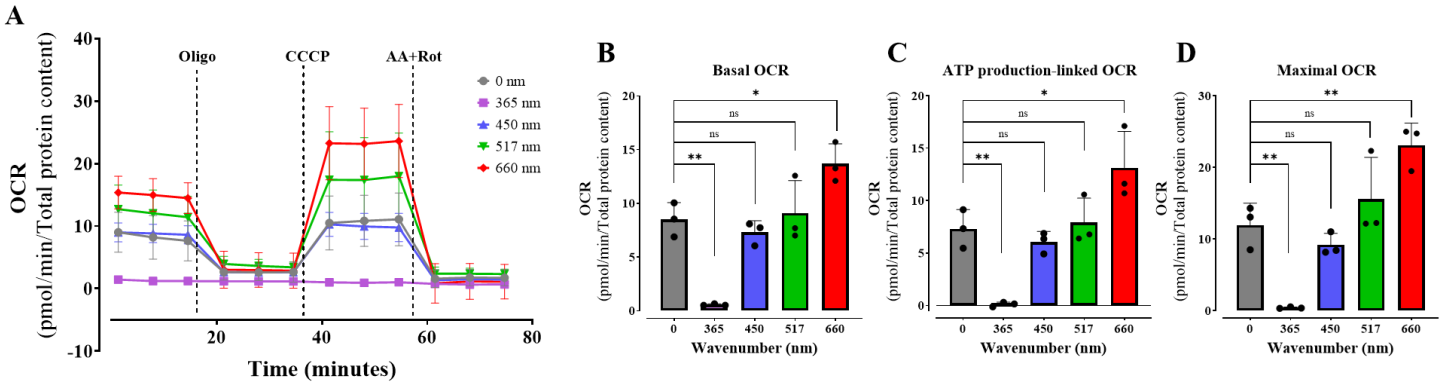

Herrera et al., Figure 2

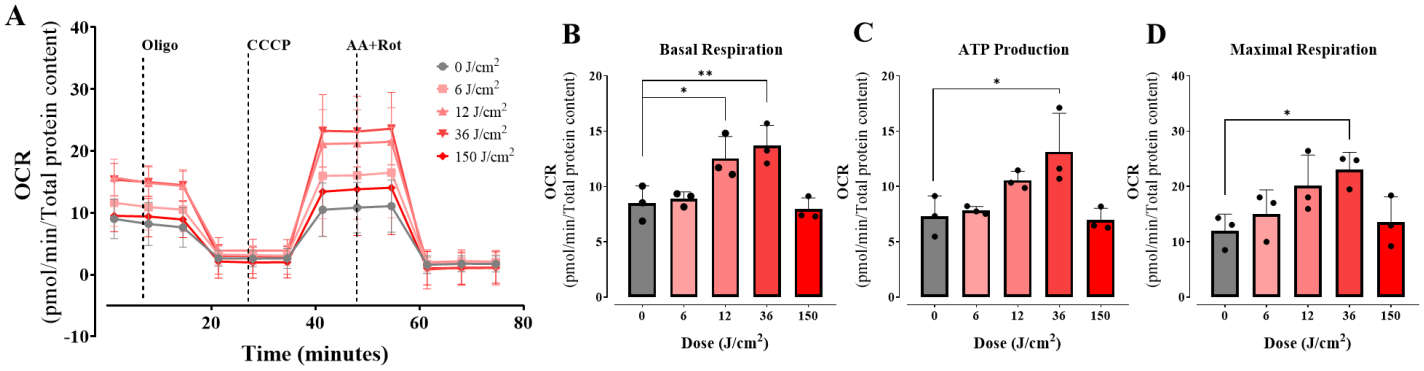

Herrera et al., Figure 3

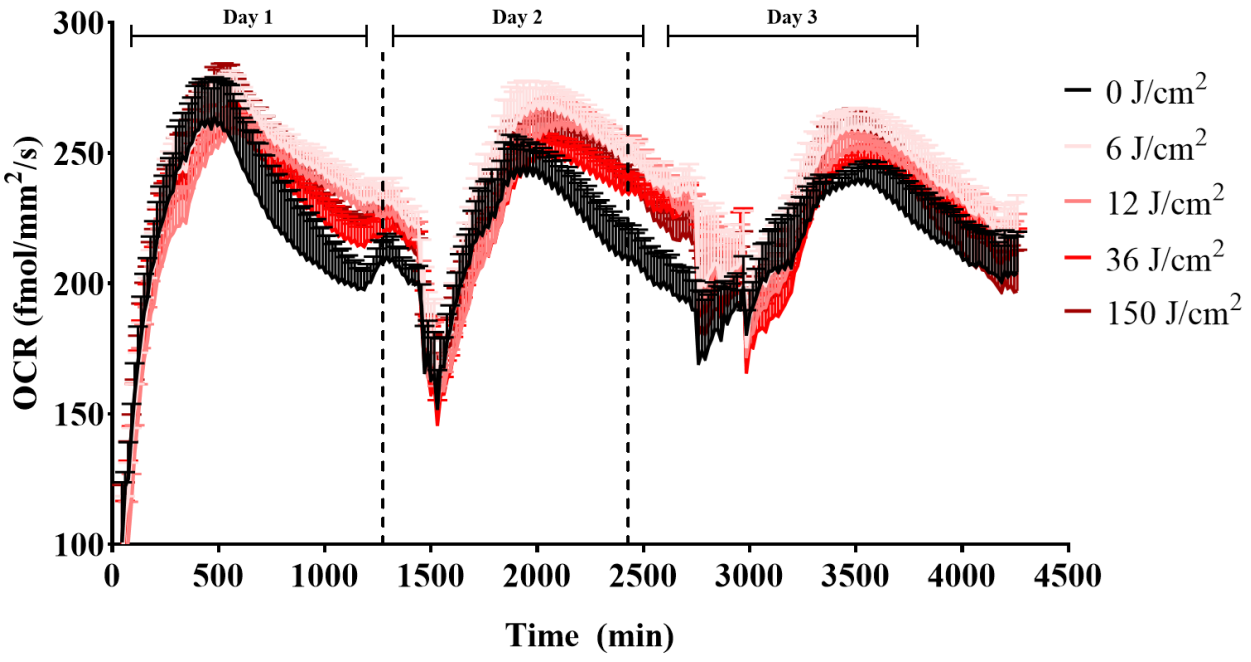

Herrera et al., Figure 4

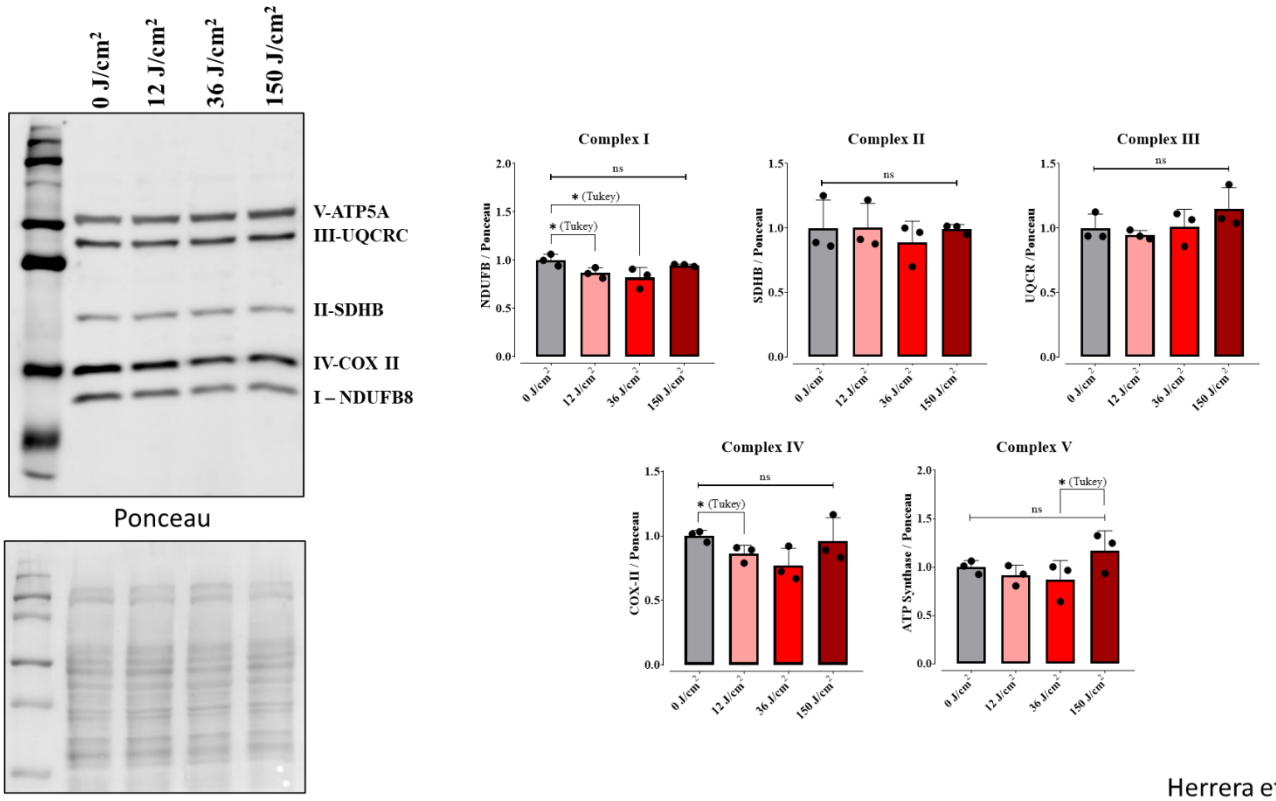

Herrera et al., Figure 5

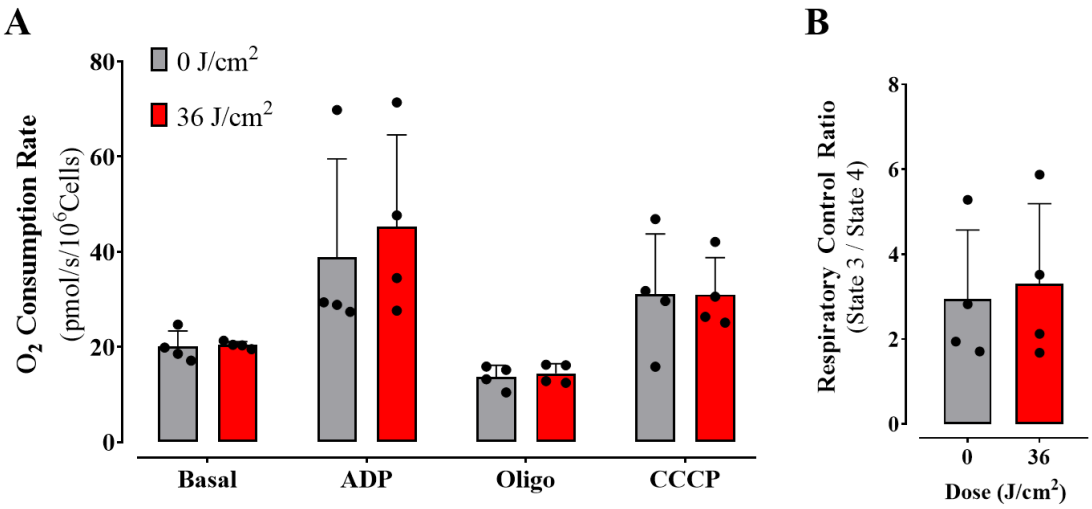

Herrera et al., Figure 6

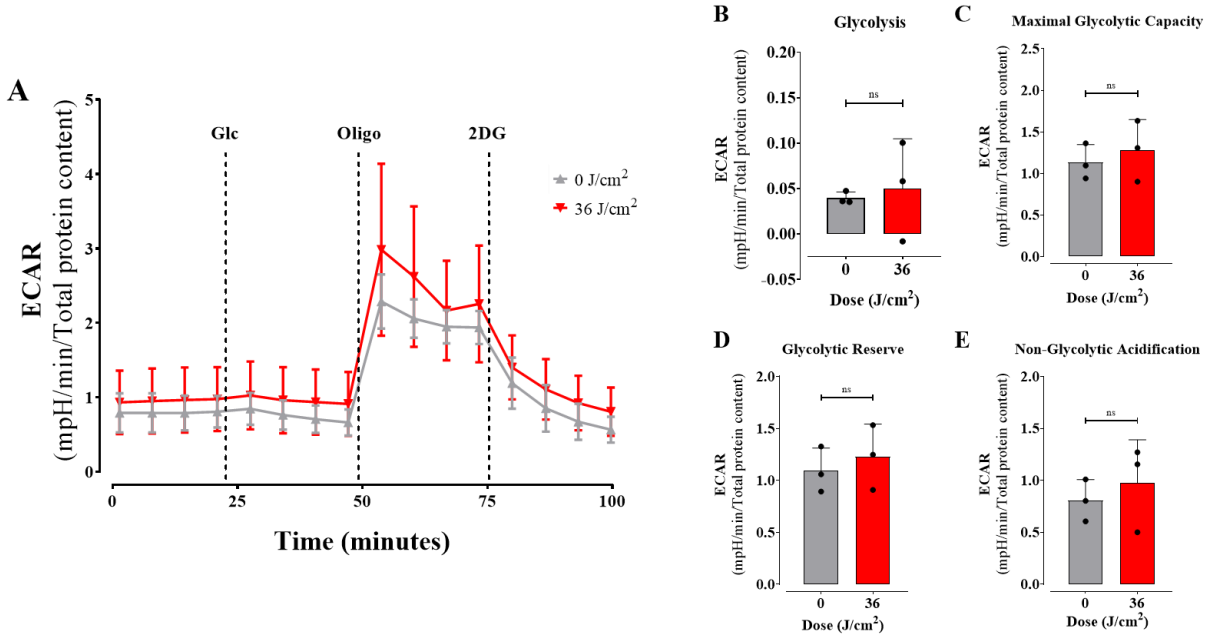

Herrera et al., Figure 7

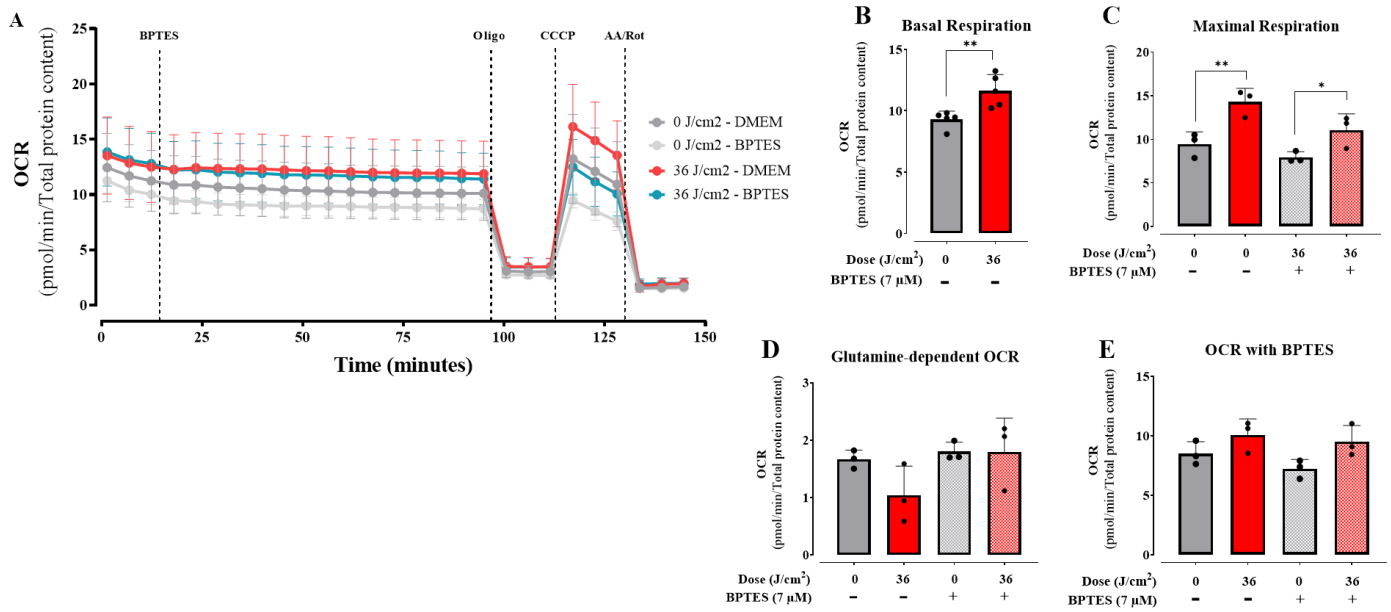

Herrera et al., Figure 8

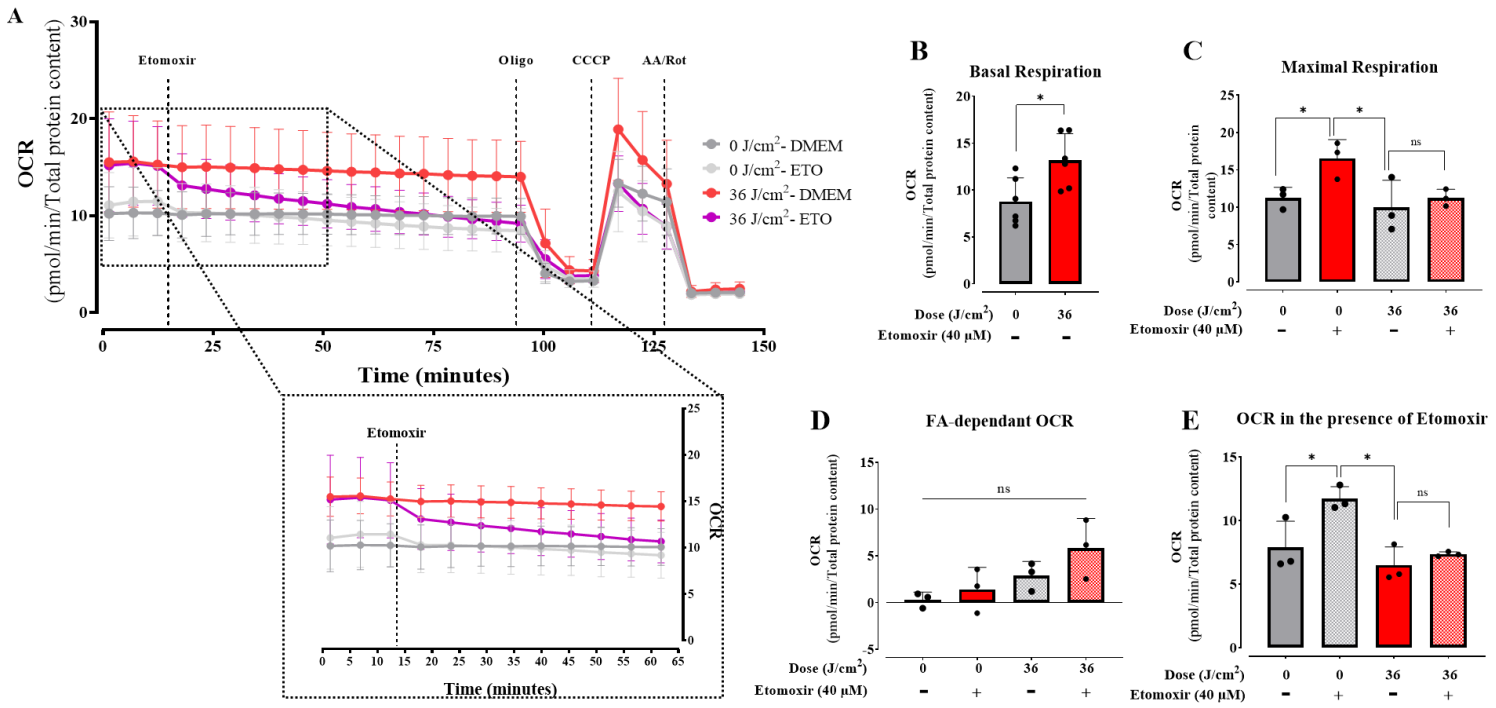

Herrera et al., Figure 9

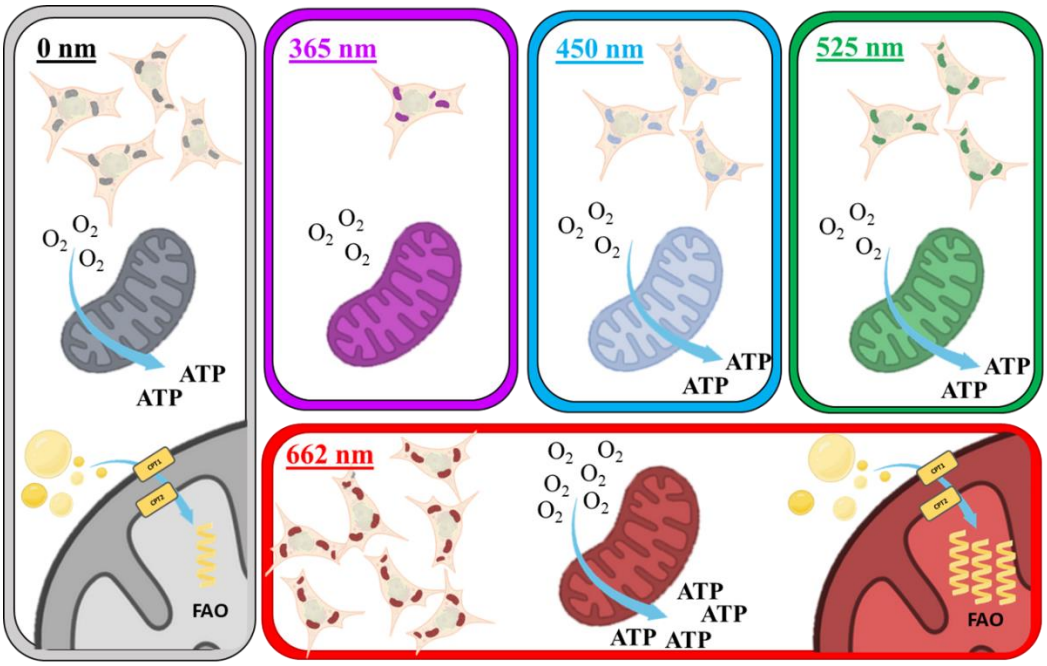

Herrera et al., Figure 10

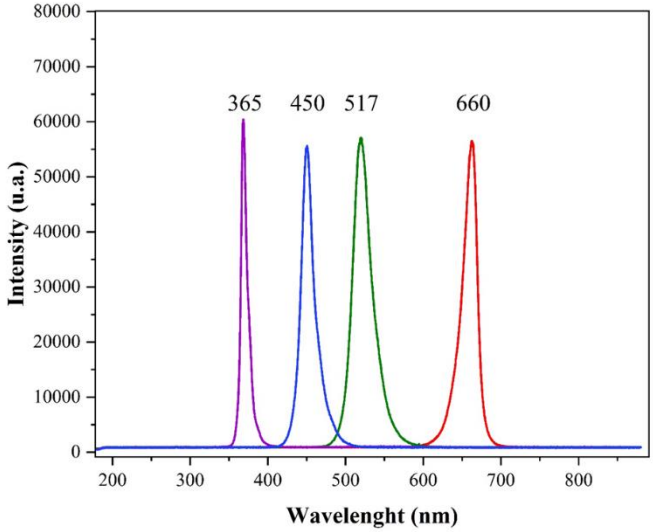

Herrera et al., Supplementary Figure S1

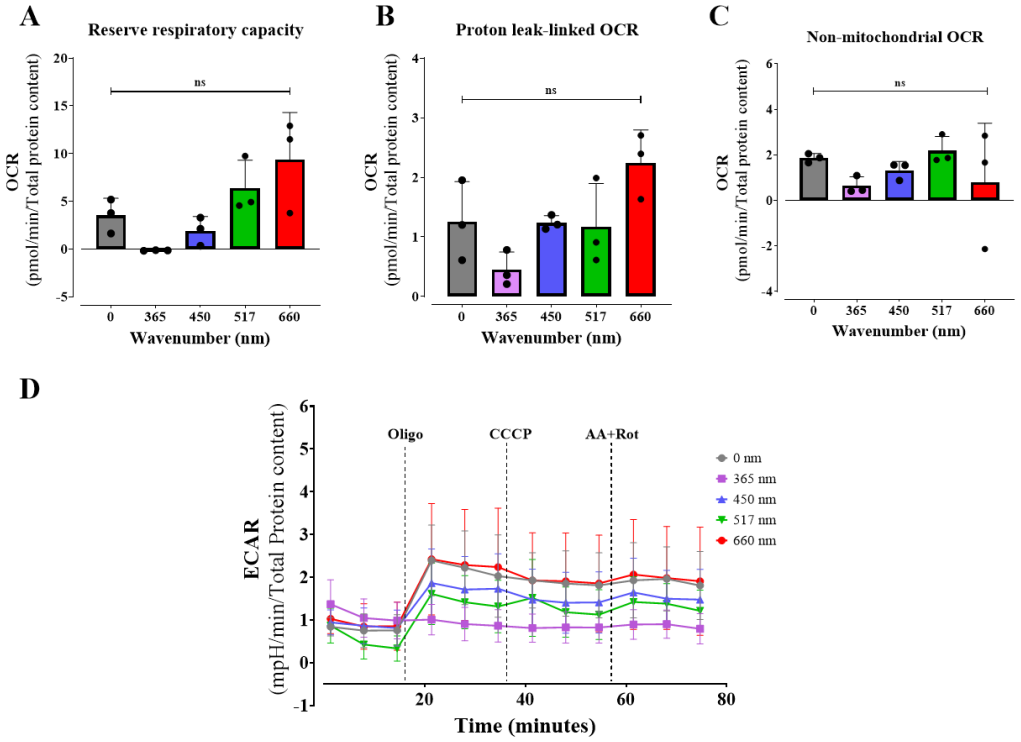

Herrera et al., Supplementary Figure S2